

1 **An antisense RNA capable of modulating the
2 expression of the tumor suppressor microRNA-34a**
3

4 **Jason T. Serviss^{1*}, Felix Clemens Richter^{1,2}, Jimmy Van Den Eynden³,**
5 **Nathanael Johansson Andrews¹, Miranda Houtman^{1,4}, Laura**
6 **Schwarzmueller¹, Per Johnsson, Erik Larsson³, Dan Grandér¹, Katja**
7 **Pokrovskaja Tamm¹**

8
9 ¹ Department of Oncology and Pathology, Karolinska Institutet, Stockholm,
10 Sweden, SE-17177

11 ² Kennedy Institute of Rheumatology, University of Oxford, Roosevelt Drive,
12 Oxford OX3 7FY, UK

13 ³Department of Medical Biochemistry and Cell Biology, Institute of
14 Biomedicine, The Sahlgrenska Academy, University of Gothenburg, SE-405
15 30 Gothenburg, Sweden

16 ⁴Rheumatology Unit, Department of Medicine, Karolinska University Hospital
17 Solna, Karolinska Institutet, Stockholm, Sweden
18 ⁵

19 * Correspondence:

20 Jason T. Serviss jason.serviss@ki.se

21 **Abstract**

22 The microRNA-34a is a well-studied tumor suppressor microRNA (miRNA)
23 that is a direct downstream target of TP53 and has roles in multiple pathways
24 associated with oncogenesis, such as proliferation, cellular growth, and
25 differentiation. Due to its wide variety of targets that suppress oncogenesis, it
26 is not surprising that miR34a expression has been shown to be dysregulated
27 in a wide variety of both solid tumors and hematological malignancies.
28 Despite this, the mechanisms by which miR34a is regulated in these cancers
29 is not well studied. Here we find that the *miR34a* antisense RNA, a long non-
30 coding RNA transcribed antisense to *miR34a*, is critical
31 for *miR34a* expression and mediation of its cellular functions in multiple types
32 of human cancer. In addition, we characterize miR34a asRNA's ability to
33 facilitate miR34a expression under multiple types of cellular stress in both

37 *TP53* deficient and wildtype settings.

38

39 **Introduction**

40 In recent years advances in functional genomics has revolutionized our
41 understanding of the human genome. Evidence now points to the fact that
42 approximately 75% of the genome is transcribed but only ~1.2% of this is
43 responsible for encoding proteins (International Human Genome Sequencing
44 2004, Djebali et al. 2012). Of these recently identified elements, long non-
45 coding (lnc) RNAs are defined as transcripts exceeding 200bp in length with a
46 lack of a functional open reading frame. Some lncRNAs are dually classified
47 as antisense (as) RNAs that are expressed from the same locus as a sense
48 transcript in the opposite orientation. Current estimates using high-throughput
49 transcriptome sequencing, indicate that up to 20-40% of the approximately
50 20,000 protein-coding genes exhibit antisense transcription (Chen et al. 2004,
51 Katayama et al. 2005, Ozsolak et al. 2010). The hypothesis that asRNAs play
52 an important role in oncogenesis was first proposed when studies increasingly
53 found examples of aberrant expression of these transcripts and other lncRNA
54 subgroups in tumor samples (Balbin et al. 2015). Although studies
55 characterizing the functional importance of asRNAs in cancer are limited to
56 date, characterization a number of individual transcripts has led to the
57 discovery of multiple examples of asRNA-mediated regulation of several well
58 known tumorigenic factors (Yap et al. 2010, Johnsson et al. 2013). The
59 mechanisms by which asRNAs accomplish this are diverse, and include
60 recruitment of chromatin modifying factors (Rinn et al. 2007), acting as
61 microRNA (miRNA) sponges (Memczak et al. 2013), and causing

62 transcriptional interference (Conley et al. 2012).

63

64 Responses to cellular stress, e.g. DNA damage, sustained oncogene
65 expression, and nutrient deprivation, are all tightly monitored and orchestrated
66 cellular pathways that are commonly dysregulated in cancer. Cellular
67 signaling in response to these types of cellular stress often converge on the
68 transcription factor TP53 that regulates transcription of coding and non-coding
69 downstream targets. One non-coding target of TP53 is the tumor suppressor

70 microRNA known as *miR34a* (Raver-Shapira et al. 2007).

71 Upon TP53 activation *miR34a* expression is increased allowing it to down-
72 regulate its targets involved in cellular pathways such as, growth factor
73 signaling, apoptosis, differentiation, and cellular senescence (Lal et al. 2011,
74 Slabakova et al. 2017). *miR34a* is a crucial factor in mediating activated TP53
75 response and it is often deleted or down-regulated in human cancers and has
76 also been shown to be a valuable prognostic marker (Cole et al. 2008,
77 Gallardo et al. 2009, Zenz et al. 2009, Cheng et al. 2010, Liu et al. 2011).

78 Reduced *miR34a* transcription is mediated via epigenetic regulation in many
79 solid tumors, such as colorectal-, pancreatic-, and ovarian cancer (Vogt et al.
80 2011), as well as multiple types of hematological malignancies (Chim et al.
81 2010). In addition, miR34a has been shown to be transcriptionally regulated
82 via TP53 homologs, TP63 and TP73, other transcription factors, e.g. STAT3
83 and MYC, and, in addition, post-transcriptionally through miRNA sponging by
84 the NEAT1 lncRNA (Chang et al. 2008, Su et al. 2010, Agostini et al. 2011,
85 Rokavec et al. 2015, Ding et al. 2017). Despite these findings, the
86 mechanisms underlying miR34a regulation in the context of oncogenesis have

87 not yet been fully elucidated.

88

89 Studies across multiple cancer types have reported a decrease in oncogenic
90 phenotypes when *miR34a* expression is induced in a p53-null background,
91 although endogenous mechanisms for achieving this have not yet been
92 discovered (Liu et al. 2011, Ahn et al. 2012, Yang et al. 2012, Stahlhut et al.
93 2015, Wang et al. 2015). In addition, previous reports from large-scale studies
94 interrogating global TP53-mediated regulation of lncRNAs have identified a
95 lncRNA originating in the antisense orientation from the *miR34a* locus which
96 is induced upon multiple forms of cellular stress (Rashi-Elkeles et al. 2014,
97 Hunten et al. 2015, Leveille et al. 2015, Ashouri et al. 2016, Kim et al.
98 2017). Despite this, none of these studies have continued to functionally
99 characterize this transcript. In this study we functionally characterize
100 the *miR34a* asRNA transcript, and find that modulating the levels of
101 the *miR34a* asRNA is sufficient to increase levels of *miR34a* and results in a
102 decrease of multiple tumorigenic phenotypes. Furthermore, we find that
103 *miR34a* asRNA-mediated up-regulation of *miR34a* is sufficient to induce
104 endogenous cellular mechanisms counteracting several types of stress stimuli
105 in a *TP53* deficient background. Finally, similar to the functional roles of
106 antisense transcription at protein-coding genes, we identify a rare example of
107 an antisense RNA capable of regulating a cancer-associated miRNA.

108

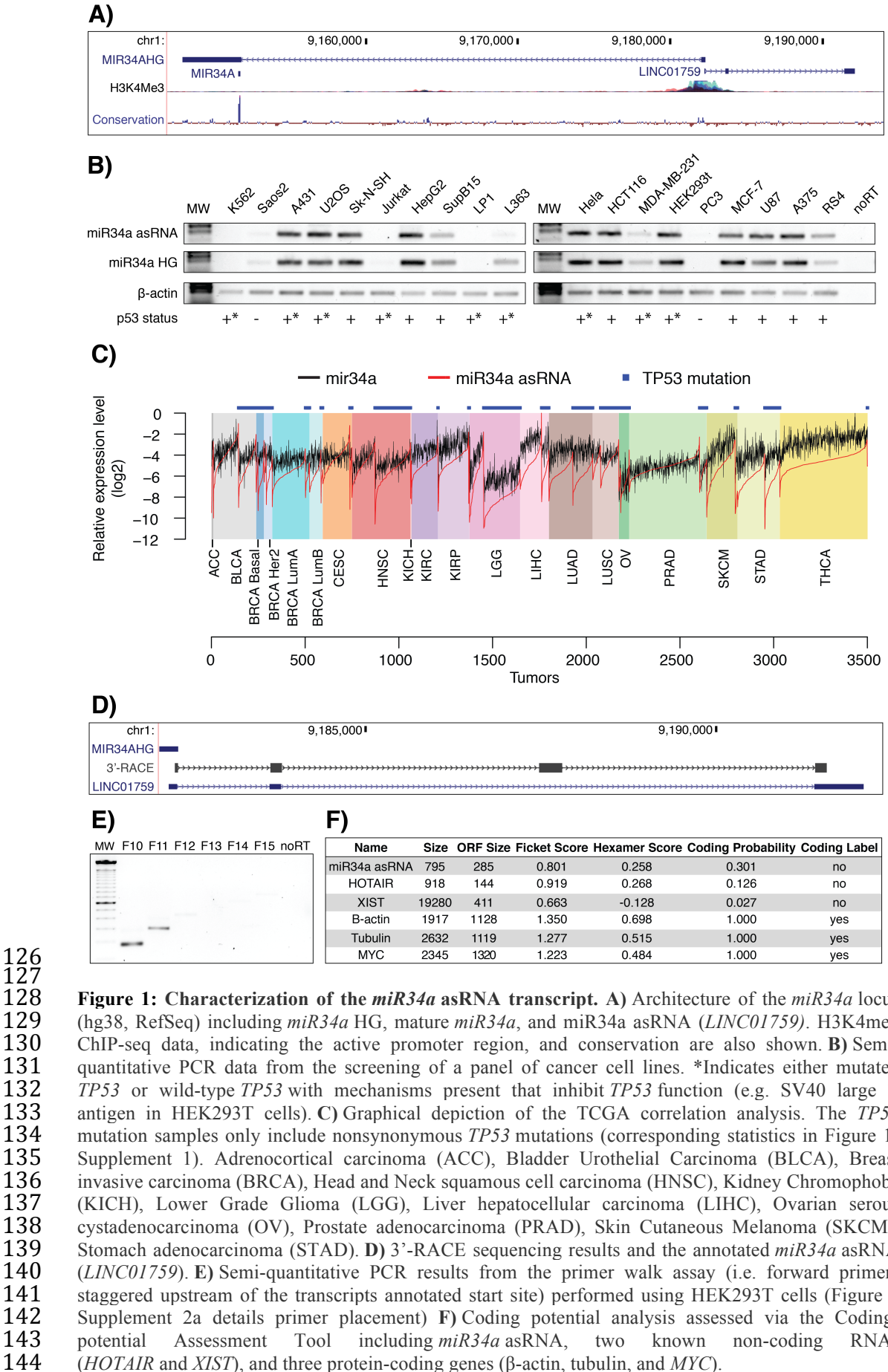
109 **Results**

110

111 ***miR34a* asRNA is a broadly expressed, non-coding transcript whose**
112 **levels correlate with *miR34a* expression**

113

114 miR34a asRNA is transcribed in a “head-to-head” orientation with
115 approximately 100 base pair overlap with the *miR34a* host gene (HG) (**Fig.**
116 **1a**). Due to the fact that sense/antisense pairs can be both concordantly and
117 discordantly expressed, we sought to evaluate this relationship in the case of
118 *miR34a* HG and its asRNA. Using a diverse panel of cancer cell lines, we
119 detected co-expression of both the *miR34a* HG and *miR34a* asRNA (**Fig. 1b**).
120 We included *TP53*+/+, *TP53* mutated, and *TP53*-/- cell lines in the panel due
121 to previous reports that *miR34a* is a known downstream target of TP53.
122 These results indicate that *miR34a* HG and *miR34a* asRNA are co-expressed
123 and that their expression levels correlate with *TP53* status, with *TP53*-/- cell
124 lines tending to have decreased or abolished expression of both transcripts.
125



145 We next sought to interrogate primary cancer samples to examine if a
146 correlation between *miR34a* asRNA and *miR34a* expression levels could be
147 identified. For this task we utilized RNA sequencing data from The Cancer
148 Genome Atlas (TCGA) after stratifying patients by cancer type, *TP53* status
149 and, where appropriate, cancer subtypes. The results indicate
150 that *miR34a* asRNA and *miR34a* expression are strongly correlated in the
151 vast majority of cancer types examined, both in the presence and absence of
152 wild-type *TP53* (**Fig. 1c, Figure 1-Figure Supplement 1a**). The results also
153 further confirm that the expression levels of both *miR34a* and its asRNA tend
154 to be reduced in patients with nonsynonymous *TP53* mutations (**Figure 1-**
155 **Figure Supplement 1b**).

156

157 Next, we aimed to gain a thorough understanding of *miR34a* asRNA's
158 molecular characteristics and cellular localization. To experimentally
159 determine the 3' termination site for the *miR34a* asRNA transcript we
160 performed 3' rapid amplification of cDNA ends (RACE) using the U2OS
161 osteosarcoma cell line that exhibited high endogenous levels
162 of *miR34a* asRNA in the cell panel screening. Sequencing the cloned cDNA
163 indicated that the transcripts 3' transcription termination site is 525 base pairs
164 upstream of the *LINC01759* transcript's annotated termination site (**Fig. 1d**).
165 Next, we characterized the *miR34a* asRNA 5' transcription start site by
166 carrying out a primer walk assay, i.e. a common reverse primer was placed in
167 exon 2 and forward primers were gradually staggered upstream of the
168 transcripts annotated start site (**Figure 1-Figure Supplement 2a**). Our results
169 indicated that the 5' start site for *miR34a* asRNA is in fact approximately 90bp

170 (F11 primer) to 220bp (F12 primer) upstream of the annotated start site (**Fig.**
171 **1e**). Polyadenylation status was evaluated via cDNA synthesis with either
172 random nanomers or oligoDT primers followed by semi-quantitative PCR with
173 results indicating that the *miR34a* asRNA is polyadenylated although the
174 unspliced form seems to only be in the polyA negative state (**Figure 1-Figure**
175 **Supplement 2b**). We furthermore investigated the propensity
176 of *miR34a* asRNA to be alternatively spliced in U2OS cells, using PCR
177 cloning and sequencing and found that the transcript is post-transcriptionally
178 spliced to form multiple different isoforms (**Figure 1-Figure Supplement 2c**).
179 Finally, to evaluate the cellular localization of *miR34a* asRNA we utilized RNA
180 sequencing data from five cancer cell lines included in the ENCODE
181 (Consortium 2012) project that had been fractionated into cytosolic and
182 nuclear fractions. The analysis revealed that the *miR34a* asRNA transcript
183 localizes to both the nucleus and cytoplasm but primarily resides in the
184 nucleus (**Figure 1-Figure Supplement 2d**).

185

186 Finally, we utilized multiple approaches to evaluate the coding potential of
187 the *miR34a* asRNA transcript. The Coding-Potential Assessment Tool is a
188 bioinformatics-based tool that uses a logistic regression model to evaluate
189 coding-potential by examining ORF length, ORF coverage, Fickett score and
190 hexamer score (Wang et al. 2013). Results indicated that *miR34a* asRNA has
191 a similar lack of coding capacity to the known non-coding
192 transcripts *HOTAIR* and *XIST* and differs greatly when examining these
193 parameters to the known coding transcripts β -actin, tubulin, and *MYC* (**Fig.**
194 **1F**). We further confirmed these results using the Coding-Potential Calculator

195 that utilizes a support based machine-based classifier and accesses an
196 alternate set of discriminatory features (**Figure 1-Figure Supplement 2e**)
197 (Kong et al. 2007). *** We hope to be able to scan for peptides matching to
198 miR34a asRNA in CPTAC and Geiger et al., 2012 before submission and will
199 mention results here.***

200

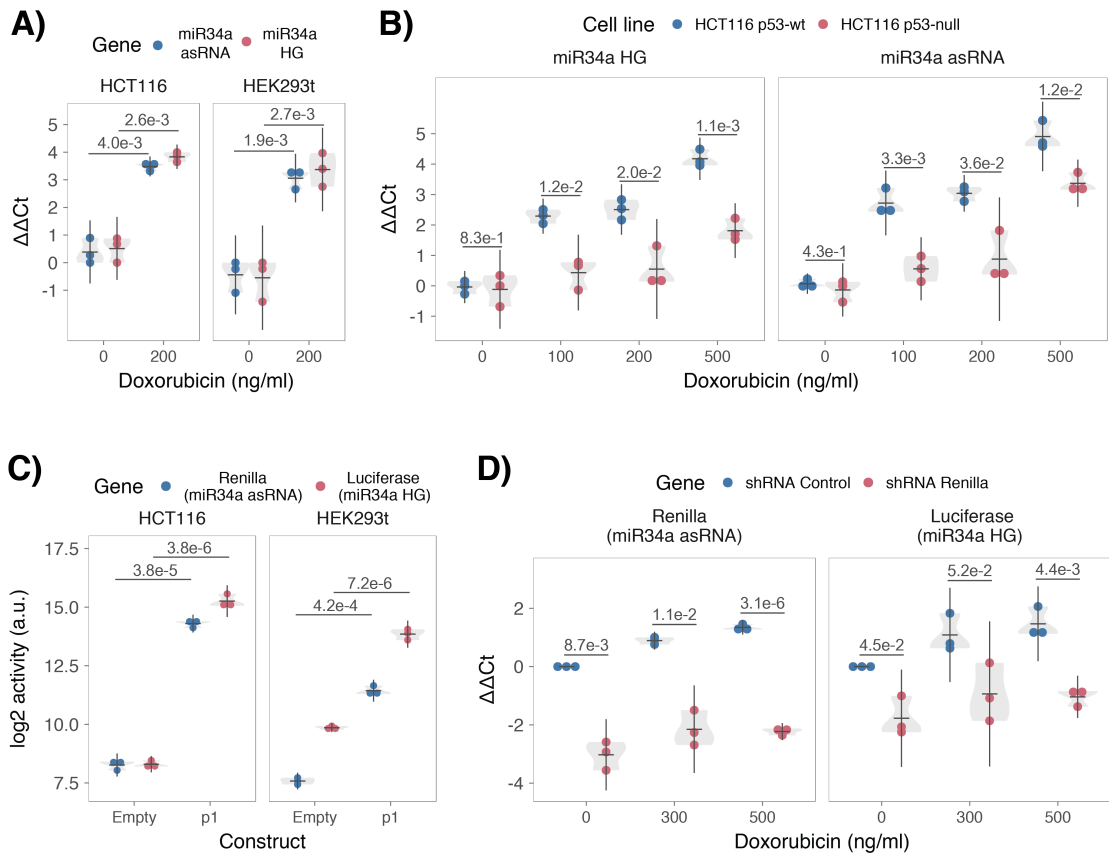
201 **TP53-mediated regulation of *miR34a* asRNA expression**

202 *miR34a* is a known downstream target of TP53 and has been previously
203 shown to exhibit increased expression within multiple contexts of cellular
204 stress. *miR34a* asRNA has also been shown to be induced upon TP53
205 activation in several global analyses of p53-regulated lncRNAs (Rashi-Elkeles
206 et al. 2014, Hunten et al. 2015, Leveille et al. 2015, Ashouri et al. 2016, Kim et
207 al. 2017). To confirm these results in our biological system, we treated
208 HEK293t, embryonic kidney cells, and HCT116, colorectal cancer cells, with
209 the DNA damaging agent doxorubicin to activate TP53. QPCR-mediated
210 measurement of both *miR34a* HG and asRNA indicated that their expression
211 levels were increased in response to doxorubicin treatment in both cell lines
212 (**Fig. 2a**). To assess if it is in fact *TP53* that is responsible for the increase
213 in *miR34a* asRNA expression upon DNA damage, we
214 treated *TP53*^{+/+} and *TP53*^{-/-} HCT116 cells with increasing concentrations of
215 doxorubicin and monitored the expression of both *miR34a* HG and asRNA.
216 We observed a dose-dependent increase in both *miR34a* HG and asRNA
217 expression levels with increasing amounts of doxorubicin, indicating that
218 these two transcripts are co-regulated, although, this effect was largely
219 abrogated in *TP53*^{-/-} cells (**Fig. 2b**). These results indicate

220 that *TP53* activation increases *miR34a* asRNA expression upon the induction
221 of DNA damage. Nevertheless, *TP53*^{-/-} cells also showed a dose dependent
222 increase in both *miR34a* HG and asRNA, indicating that additional factors,
223 other than *TP53*, are capable of initiating an increase in expression of both of
224 these transcripts upon DNA damage.

225

226



227

Figure 2: TP53-mediated regulation of the *miR34a* locus. **A)** Evaluating the effects of 24 hours of treatment with 200 ng/ml doxorubicin on *miR34a* asRNA and HG in HCT116 and HEK293t cells.* **B)** Monitoring *miR34a* HG and asRNA expression levels during 24 hours doxorubicin treatment in *TP53*^{+/+} and *TP53*^{-/-} HCT116 cells.* **C)** Quantification of luciferase and renilla levels after transfection of HCT116 and HEK293T cells with the p1 construct (Figure 2 Supplement 2 contains a schematic representation of the p1 construct).* **D)** HCT116 cells were co-transfected with the p1 construct and shRNA renilla or shRNA control and subsequently treated with increasing doses of doxorubicin. 24 hours post-treatment, cells were harvested and renilla and luciferase levels were measured using QPCR. Resulting p-values from statistical testing are shown above the shRenilla samples which were compared to the shRNA control using the respective treatment condition.* Individual points represent results from independent experiments and the gray shadow indicates the density of those points. Error bars show the 95% CI, black horizontal lines represent the mean, and p-values are shown over long horizontal lines indicating the comparison tested. All experiments in Figure 2 were performed biological triplicate.

228

229

230

231

232

233

234

235

236

237

238

239

240

241

242 The head-to head orientation of *miR34a* HG and asRNA, suggests that
243 transcription is initiated from a single promoter in a bi-directional manner. To
244 investigate whether *miR34a* HG and asRNA are transcribed from the same
245 promoter as divergent transcripts, we cloned the previously reported
246 *miR34a* HG promoter, including the *TP53* binding site, into a luciferase/renilla
247 dual reporter vector which we hereafter refer to as p1 (**Figure 2-Figure**
248 **Supplement 1a-b**) (Raver-Shapira et al. 2007). Upon transfection of p1 into
249 HCT116 and HEK293t cell lines we observed increases in both luciferase and
250 renilla indicating that *miR34a* HG and asRNA expression can be regulated by
251 a single promoter contained within the p1 construct (**Fig. 2c**).
252

253 We hypothesized that *miR34a* asRNA may regulate *miR34a* HG levels and, in
254 addition, that the overlapping regions of the sense and antisense transcripts
255 may have a crucial role in mediating this regulation. Knockdown of
256 endogenous *miR34a* asRNA is complicated by its various isoforms (**Figure 1-**
257 **Figure Supplement 2c**). For this reason, we utilized the p1 construct to
258 evaluate the regulatory role of the miR34a asRNA on miR34a HG.
259 Accordingly, we first co-transfected the p1 construct, containing the
260 overlapping region of the two transcripts, and two different short hairpin (sh)
261 RNAs targeting renilla into HEK293T cells and subsequently measured
262 luciferase and renilla expression. The results indicated that shRNA-mediated
263 knock down of the p1-renilla transcript (corresponding to *miR34a* asRNA)
264 caused p1-luciferase (corresponding to *miR34a* HG) levels to concomitantly
265 decrease (**Figure 2-Figure Supplement 2**). These results indicate
266 that *miR34a* asRNA positively regulates levels of *miR34a* HG and that the

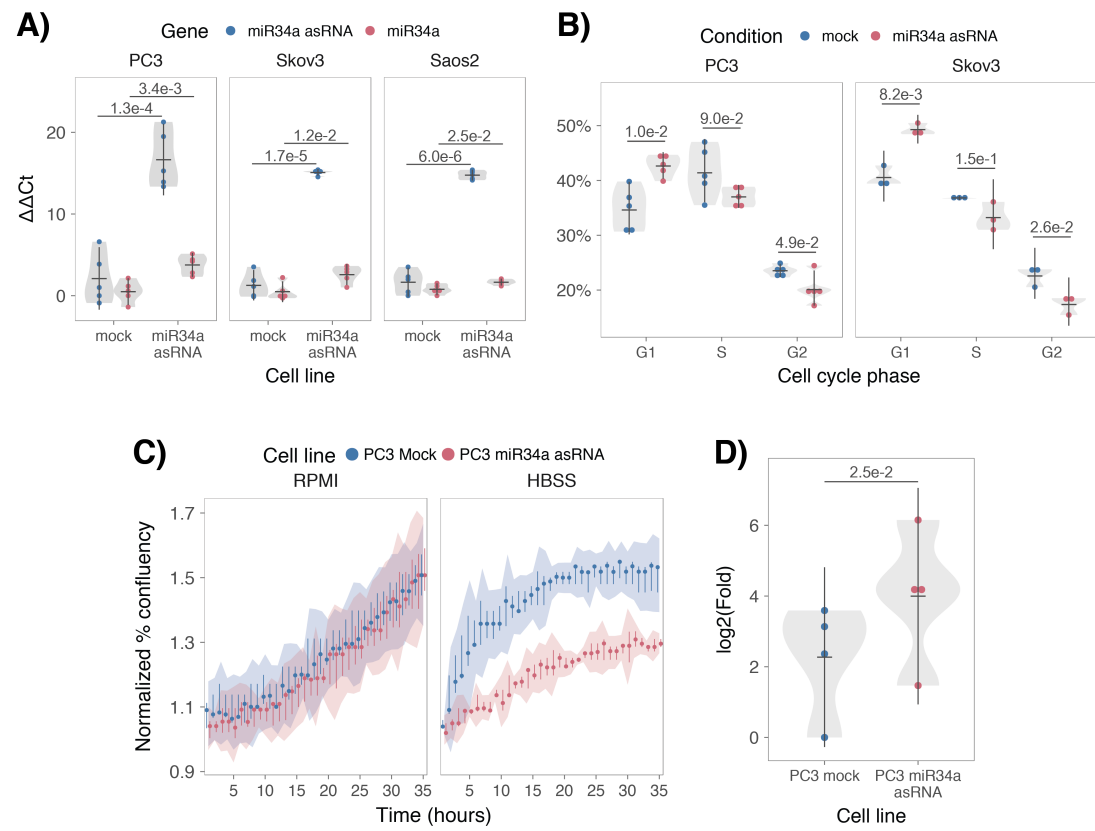
267 transcriptional product of the *miR34a* asRNA within in the p1 construct
268 promotes a miR34a response. To further support these conclusions and
269 better understand the role of miR34a asRNA during TP53 activation, *TP53^{+/+}*
270 HCT116 cells were co-transfected with p1 and shRNA renilla (2.1) and
271 subsequently treated with increasing doses of doxorubicin. Again, the results
272 showed a concomitant reduction in luciferase levels upon knock-down of p1-
273 renilla i.e. the *miR34a* asRNA corresponding segment of the p1 transcript
274 (**Fig. 2d**). Furthermore, the results showed that in the absence of p1-renilla
275 the expected induction of p1-luciferase in response to TP53 activation to DNA
276 damage is abrogated. Collectively these results indicate that *miR34a* asRNA
277 positively regulates *miR34a* expression and is crucial for an appropriate
278 TP53-mediated *miR34a* response to DNA damage.

279

280 ***miR34a* asRNA regulates its host gene independently of TP53**
281 Despite the fact that TP53 regulates *miR34a* HG and asRNA expression, our
282 results indicated that other factors are also able to regulate this locus (**Fig.**
283 **2b**). Utilizing a lentiviral system, we stably over-expressed the *miR34a* asRNA
284 transcript in three *TP53*-null cell lines, PC3 (prostate cancer), Saos2
285 (osteogenic sarcoma), and Skov3 (ovarian adenocarcinoma). We first
286 analyzed the levels of *miR34a* asRNA in these stable over-expression cell
287 lines, compared to HEK293T cells, which have high endogenous levels
288 of *miR34a* asRNA, finding that, on average, the over-expression was
289 approximately 30-fold higher in the over-expression cell lines than in HEK293t
290 cells. Due to the fact that *miR34a* asRNA can be up-regulated ~30-fold in
291 response to DNA damage (**Fig. 2b**), we deemed this over-expression level to

292 correspond to physiologically relevant levels in cells encountering a stress
293 stimulus, such as DNA damage (**Figure 3-Figure Supplement 1**). Analysis
294 of *miR34a* levels in the *miR34a* asRNA over-expressing cell lines showed that
295 this over-expression resulted in a concomitant increase in the expression
296 of *miR34a* in all three cell lines (**Fig. 3a**). These results indicate that, in the
297 absence of *TP53*, *miR34a* expression may be rescued by increasing the
298 levels of *miR34a* asRNA expression.

299



300 **Figure 3: miR34a asRNA positively regulates miR34a and its associated phenotypes.** **A)** QPCR-
301 mediated quantification of miR34a expression in cell lines stably over-
302 expressing miR34a asRNA.* **B)** Cell cycle analysis comparing stably over-expressing miR34a asRNA
303 cells to the respective mock expressing cells.* **C)** Analysis of cellular growth over time in miR34a
304 asRNA over-expressing PC3 cells. Points represent the median from 3 independent experiments, the
305 colored shadows indicate the 95% confidence interval, and vertical lines show the minimum and
306 maximum values obtained from the three biological replicates. **D)** Differential phosphorylated
307 polymerase II binding in miR34a asRNA over-expressing PC3 cells.* *Individual points represent
308 results from independent experiments and the gray shadow indicates the density of those points. Error
309 bars show the 95% CI, black horizontal lines represent the mean, and p-values are shown over long
310 horizontal lines indicating the comparison tested.
311

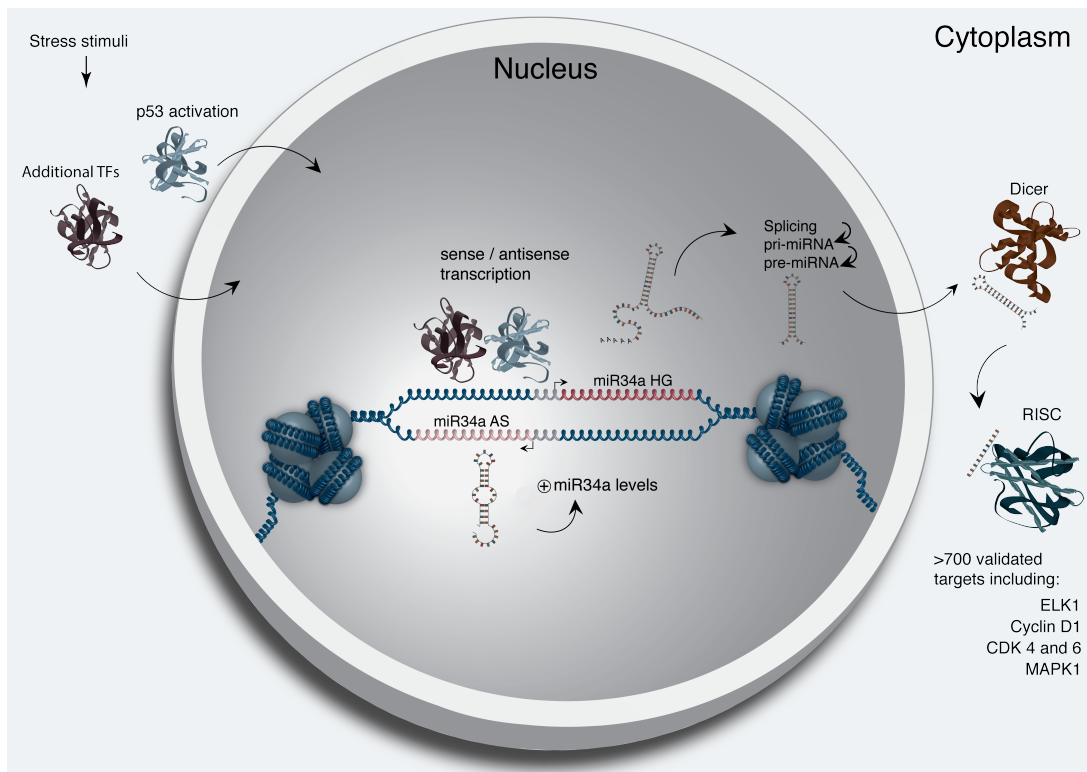
312 *miR34a* has been previously shown to regulate cell cycle progression, with
313 *miR34a* induction causing G1 arrest (Raver-Shapira et al. 2007, Tarasov et al.
314 2007). Cell cycle analysis via determination of DNA content showed a
315 significant increase in G1 phase cells in the PC3 and Skov3 *miR34a* asRNA
316 over-expressing cell lines, indicative of G1 arrest, as well as, a significant
317 decrease of cells in G2 phase (**Fig. 3b**). *miR34a*'s effects on the cell cycle are
318 mediated by its ability to target cell cycle regulators such as cyclin D1
319 (*CCND1*) (Sun et al. 2008). We therefore sought to determine if
320 the *miR34a* asRNA over-expressing cell lines exhibited effects on this
321 known *miR34a* target. Quantification of both *CCND1* RNA expression (**Figure**
322 **3-Figure Supplement 2a**) and protein levels (**Figure 3-Figure Supplement**
323 **2b**) in the PC3 *miR34a* asRNA over-expressing cell line showed a significant
324 decrease of *CCND1* levels compared to the mock control.

325
326 *miR34a* is also a well known inhibitor of cellular growth via its ability to
327 negatively regulate growth factor signaling. Furthermore, starvation has been
328 shown to induce *miR34a* expression that down-regulates multiple targets that
329 aid in the phosphorylation of pro-survival growth factors (Lal et al. 2011). We
330 further interrogated the effects of *miR34a* asRNA over-expression by
331 monitoring the growth of the cells in both normal and starvation conditions via
332 confluency measurements over a 35-hour period. Under normal growth
333 conditions there is a small but significant reduction ($p = 3.0\text{e-}8$) in confluency
334 in the *miR34a* asRNA over-expressing cell lines although, these effects on
335 cell growth are drastically increased in starvation conditions ($p = 9.5\text{e-}67$).
336 This is in accordance with our previous results, and suggests

337 that *miR34a* asRNA-mediated increases in *miR34a* expression are crucial
338 under conditions of stress and necessary for the initiation of an appropriate
339 cellular response. In summary, we find that over-expression
340 of *miR34a* asRNA is sufficient to increase *miR34a* expression and gives rise
341 to known phenotypes observed with induction of *miR34a*.

342

343 Antisense RNAs have been reported to mediate their effects both via
344 transcriptional and post-transcriptional mechanisms. Due to the fact that
345 *miR34a* expression is undetected in wild type PC3 cells but, upon over-
346 expression of *miR34a* asRNA, increases to detectable levels, we
347 hypothesized that *miR34a* asRNA is capable of regulating *miR34a* expression
348 via a transcriptional mechanism. To ascertain if this is actually the case, we
349 performed chromatin immunoprecipitation (ChIP) for phosphorylated
350 polymerase II (polII) at the *miR34a* HG promoter in both *miR34a* asRNA over-
351 expressing and mock control cell lines. Our results indicated a clear increase
352 in phosphorylated polII binding at the *miR34a* promoter upon *miR34a* asRNA
353 over-expression indicating the ability of *miR34a* asRNA to regulate *miR34a*
354 levels on a transcriptional level (**Fig. 3d**).



355

356 **Figure 4: A graphical summary of the proposed *miR34a* asRNA function.** Stress stimuli,
357 originating in the cytoplasm or nucleus, activates *TP53* as well as additional factors. These factors then
358 bind to the *miR34a* promoter and drive transcription of the sense and antisense strands. *miR34a* asRNA
359 serves to increase the levels of *miR34a* HG transcription via an unknown mechanism. *miR34a* HG
360 then, in turn, is then spliced, processed by the RNase III enzyme Drosha, and exported to the
361 cytoplasm. The *miR34a* pre-miRNA then binds to Dicer where the hair-pin loop is cleaved and
362 mature *miR34a* is formed. Binding of the mature *miR34a* miRNA to the RISC complex then allows it
363 to bind and repress its targets.

364 **Discussion**

365
366 Multiple studies have previously shown asRNAs to be crucial for the
367 appropriate regulation of cancer-associated protein-coding genes and that
368 their dys-regulation can lead to perturbation of tumor suppressive and
369 oncogenic pathways, as well as, cancer-related phenotypes (Yu et al. 2008,
370 Yap et al. 2010, Serviss et al. 2014, Balbin et al. 2015). Here we show that
371 asRNAs are also capable of regulating cancer-associated miRNAs resulting in
372 similar consequences as protein-coding gene dys-regulation (**Fig. 4**).
373 Interestingly, we show that, both in the presence and absence of
374 *TP53*, *miR34a* asRNA provides an additional regulatory level and functions by
375 mediating the increase of *miR34a* expression in both homeostasis and upon
376 encountering multiple forms of cellular stress. Furthermore, we find that
377 *miR34a* asRNA-mediated increases in *miR34a* expression levels are sufficient
378 to drive the appropriate cellular responses to multiple forms of stress stimuli
379 that are encountered (**Fig. 2d and Fig. 3c**). Previous studies have utilized
380 various molecular methods to up regulate *miR34a* expression in a p53
381 deficient background showing similar phenotypic outcomes but, to our
382 knowledge, this is the first example of an endogenous mechanism by which
383 this can be achieved (Liu et al. 2011, Ahn et al. 2012, Yang et al. 2012,
384 Stahlhut et al. 2015, Wang et al. 2015).

385

386 In agreement with previous studies, we demonstrate that upon encountering
387 various types of cellular stress, TP53 in concert with additional factors bind
388 and initiate transcription at the *miR34a* locus, thus increasing the levels of
389 *miR34a* and, in addition, *miR34a* asRNA. We hypothesize that *miR34a*

390 asRNA may provide positive feedback for *miR34a* expression whereby
391 *miR34a* asRNA serves as a scaffold for the recruitment of additional factors
392 that facilitate polymerase II-mediated transcription, thus, increasing the
393 expression of *miR34a* and driving the cell towards a reduction in growth factor
394 signaling, senescence, and eventually apoptosis. On the other hand, in cells
395 without functional *TP53*, other factors, which typically act independently or in
396 concert with *TP53*, may initiate transcription of the *miR34a* locus. We believe
397 that *miR34a* asRNA could potentially be interacting directly with one of these
398 additional factors and recruiting it to the *miR34a* locus in order to drive
399 *miR34a* transcription. This is especially plausible due to head-to-head
400 orientation of the *miR34a* HG and asRNA, causing sequence complementarity
401 between the RNA and the promoter DNA. Previous reports have also
402 illustrated the ability of asRNAs to form hybrid DNA:RNA R-loops and, thus,
403 facilitate an open chromatin structure and the transcription of the sense gene
404 (Boque-Sastre et al. 2015). The fact that the p1 construct only contains a
405 small portion of the *miR34a* asRNA transcript indicates that this portion is
406 sufficient to give rise to at least a partial *miR34a* inducing response and
407 therefore, indicates that *miR34a* asRNA may be able to facilitate *miR34a*
408 expression independent of additional factors (**Fig 2d, Figure 2-Figure**
409 **Supplement 2a**). Nevertheless, further work will need to be performed to
410 ascertain the mechanism that is utilized in the case of *miR34a* asRNA.

411

412 An antisense transcript arising from the *miR34a* locus, *Lnc34a*, has been
413 previously reported to negatively regulate the expression of *miR34a* (Wang et
414 al. 2016). Although the *Lnc34a* and *miR34a* asRNA transcripts share some

415 sequence similarity, we believe them to be separate RNAs that are,
416 potentially, different isoforms of the same gene. We thoroughly address our
417 reasons for these beliefs and give appropriate supporting evidence in
418 (**Supplementary Document 1**). The fact that *Lnc34a* and *miR34a* asRNA
419 would appear to have opposing roles in their regulation of *miR34a* further
420 underlines the complexity of the regulation at this locus.

421

422 Clinical trials utilizing *miR34a* replacement therapy have previously been
423 conducted but, disappointingly, were terminated after adverse side effects of
424 an immunological nature were observed in several of the patients (Slabakova
425 et al. 2017). Although it is not presently clear if these side effects were caused
426 by *miR34a* or the liposomal carrier used to deliver the miRNA, the multitude of
427 evidence indicating *miR34a*'s crucial role in oncogenesis still makes its
428 therapeutic induction an interesting strategy for therapy and needs further
429 investigation. In summary, our results indicate that *miR34a* asRNA is a vital
430 player in the regulation of *miR34a* and is especially important in typical
431 examples of cellular stress encountered in cancer. We believe the
432 conclusions drawn in this study to be essential in the progress towards
433 developing a better understanding of the regulation of cancer-associated
434 miRNAs and, specifically, the tumor suppressor *miR34a*.

435

436 **Materials and Methods**

437 **Cell Culture**

438 All cell lines were cultured at 5% CO₂ and 37° C with HEK293T, Saos2, and
439 Skov3 cells cultured in DMEM high glucose (GE Healthcare Life Sciences,

440 Hyclone, Amersham, UK, Cat# SH30081), HCT116 and U2OS cells in
441 McCoy's 5a (ThermoFisher Scientific, Pittsburgh, MA, USA. Cat# SH30200),
442 and PC3 cells in RPMI (GE Healthcare Life Sciences, Hyclone, Cat#
443 SH3009602) and 2 mM L-glutamine (GE Healthcare Life Sciences, Hyclone,
444 Cat# SH3003402). All growth mediums were supplemented with 10% heat-
445 inactivated FBS (ThermoFisher Scientific, Gibco, Cat# 12657029) and 50
446 µg/ml of streptomycin (ThermoFisher Scientific, Gibco, Cat# 15140122) and
447 50 µg/ml of penicillin (ThermoFisher Scientific, Gibco, Cat# 15140122). All cell
448 lines were purchased from ATCC, tested negative for mycoplasma, and their
449 identity was verified via STR profiling.

450

451 **Bioinformatics, Data Availability, and Statistical Testing**

452 The USCS genome browser (Kent et al. 2002) was utilized for the
453 bioinformatic evaluation of antisense transcription utilizing the RefSeq
454 (O'Leary et al. 2016) gene annotation track.

455

456 All raw experimental data, code used for analysis, and supplementary
457 methods are available for review at ([Serviss 2017](#)) and are provided as an R
458 package. All analysis took place using the R statistical programming language
459 (Team 2017) using multiple external packages that are all documented in the
460 package associated with the article (Wilkins , Chang 2014, Wickham 2014,
461 Wickham 2016, Allaire et al. 2017, Arnold 2017, Wickham 2017, Wickham
462 2017, Wickham 2017, Xiao 2017, Xie 2017). The package facilitates
463 replication of the operating system and package versions used for the original
464 analysis, reproduction of each individual figure and figure supplement
465 included in the article, and easy review of the code used for all steps of the

466 analysis, from raw-data to figure.

467

468 The significance threshold (alpha) in this study was set to 0.05. Statistical
469 testing was performed using a two sample Student's t-test unless otherwise
470 specified.

471

472 **Coding Potential**

473 Protein-coding capacity was evaluated using the Coding-potential
474 Assessment Tool (Wang et al. 2013) and Coding-potential Calculator (Kong et
475 al. 2007) with default settings. Transcript sequences for use with Coding-
476 potential Assessment Tool were downloaded from the UCSC genome
477 browser using the Ensembl
478 accessions: *HOTAIR* (ENST00000455246), *XIST* (ENST00000429829), β-
479 actin (ENST00000331789), Tubulin (ENST00000427480),
480 and *MYC* (ENST00000377970). Transcript sequences for use with Coding-
481 potential Calculator were downloaded from the UCSC genome browser using
482 the following IDs: *HOTAIR* (uc031qho.1), β-actin (uc003sqq.4).

483

484 **shRNAs**

485 shRNA-expressing constructs were cloned into the U6M2 construct using the
486 BgIII and KpnI restriction sites as previously described (Amarzguioui et al.
487 2005). shRNA constructs were transfected using Lipofectamine 2000 or 3000
488 (ThermoFisher Scientific, Cat# 12566014 and L3000015). The sequences
489 targeting renilla is as follows: shRenilla 1.1 (AAT ACA CCG CGC TAC TGG
490 C), shRenilla 2.1 (TAA CGG GAT TTC ACG AGG C).

491 **Bi-directional Promoter Cloning**

492 The overlapping region (p1) corresponds with the sequence previously
493 published as the TP53 binding site in (Raver-Shapira et al. 2007) which we
494 synthesized, cloned into the pLucRluc construct (Polson et al. 2011) and
495 sequenced to verify its identity.

496

497 **Promoter Activity**

498 Cells were co-transfected with the renilla/firefly bidirectional promoter
499 construct (Polson et al. 2011) and GFP by using Lipofectamine 2000 (Life
500 Technologies, Cat# 12566014). The expression of GFP and luminescence
501 was measured 24 h post transfection by using the Dual-Glo Luciferase Assay
502 System (Promega, Cat# E2920) and detected by the GloMax-Multi+ Detection
503 System (Promega, Cat# SA3030). The expression of luminescence was
504 normalized to GFP.

505

506 **Generation of U6-expressed miR34a AS Lentiviral Constructs**

507 The U6 promoter was amplified from the U6M2 cloning plasmid (Amarzguioui
508 et al. 2005) and ligated into the Not1 restriction site of the pHIV7-IMPDH2
509 vector (Turner et al. 2012). miR43a asRNA was PCR amplified and
510 subsequently cloned into the Nhe1 and Pac1 restriction sites in the pHIV7-
511 IMPDH2-U6 plasmid.

512

513 **Lentiviral Particle production, infection, and selection**

514 Lentivirus production was performed as previously described in (Turner et al.
515 2012). Briefly, HEK293T cells were transfected with viral and expression

516 constructs using Lipofectamine 2000 (ThermoFisher Scientific, Cat#
517 12566014), after which viral supernatants were harvested 48 and 72 hours
518 post-transfection. Viral particles were concentrated using PEG-IT solution
519 (Systems Biosciences, Palo Alto, CA, USA. Cat# LV825A-1) according to the
520 manufacturer's recommendations. HEK293T cells were used for virus titration
521 and GFP expression was evaluated 72hrs post-infection via flow cytometry
522 (LSRII, BD Biosciences, San Jose, CA, USA) after which TU/ml was
523 calculated.

524

525 Stable lines were generated by infecting cells with a multiplicity of infection of
526 1 after which 1-2 µM mycophenolic acid (Merck, Kenilworth, NJ, USA. Cat#
527 M5255) selection was initiated 48 hours post-infection. Cells were expanded
528 as the selection process was monitored via flow cytometry analysis (LSRII,
529 BD Biosciences) of GFP and selection was terminated once > 90% of the
530 cells were GFP positive. Quantification of *miR34a* asRNA over-expression
531 and *miR34a* was performed in biological quintuplet for all cell lines.

532

533 **Western Blotting**

534 Samples were lysed in 50 mM Tris-HCl (Sigma Aldrich, St. Louis, MO, USA.
535 Cat# T2663), pH 7.4, 1% NP-40 (Sigma Aldrich, Cat# I8896), 150 mM NaCl
536 (Sigma Aldrich, Cat# S5886), 1 mM EDTA (Promega, Madison, WI, USA.
537 Cat# V4231), 1% glycerol (Sigma Aldrich, Cat# G5516), 100 µM vanadate
538 (Sigma Aldrich, Cat# S6508), protease inhibitor cocktail (Roche Diagnostics,
539 Basel, Switzerland, Cat# 004693159001) and PhosSTOP (Roche
540 Diagnostics, Cat# 04906837001). Lysates were subjected to SDS-PAGE and

541 transferred to PVDF membranes. The proteins were detected by western blot
542 analysis by using an enhanced chemiluminescence system (Western
543 Lightning-ECL, PerkinElmer, Waltham, MA, USA. Cat# NEL103001EA).
544 Antibodies used were specific for *CCND1* 1:1000 (Cell Signaling, Danvers,
545 MA, USA. Cat# 2926), and β-actin 1:5000 (Sigma-Aldrich, Cat# A5441). All
546 western blot quantifications were performed using ImageJ (Schneider et al.
547 2012).

548

549 **RNA Extraction and cDNA Synthesis**

550 For downstream SYBR green applications, RNA was extracted using the
551 RNeasy mini kit (Qiagen, Venlo, Netherlands, Cat# 74106) and subsequently
552 treated with DNase (Ambion Turbo DNA-free, ThermoFisher Scientific, Cat#
553 AM1907). 500ng RNA was used for cDNA synthesis using MuMLV
554 (ThermoFisher Scientific, Cat# 28025013) and a 1:1 mix of oligo(dT) and
555 random nanomers.

556

557 For analysis of miRNA expression with Taqman, samples were isolated with
558 TRIzol reagent (ThermoFisher Scientific, Cat# 15596018) and further
559 processed with the miRNeasy kit (Qiagen, Cat# 74106). cDNA synthesis was
560 performed using the TaqMan MicroRNA Reverse Transcription Kit
561 (ThermoFisher Scientific, Cat# 4366597) using the corresponding oligos
562 according to the manufacturer's recommendations.

563

564 **QPCR and PCR**

565 PCR was performed using the KAPA2G Fast HotStart ReadyMix PCR Kit

566 (Kapa Biosystems, Wilmington, MA, USA, Cat# KK5601) with corresponding
567 primers. QPCR was carried out using KAPA 2G SYBRGreen (Kapa
568 Biosystems, Cat# KK4602) using the Applied Biosystems 7900HT machine
569 with the cycling conditions: 95 °C for 3 min, 95 °C for 3 s, 60 °C for 30 s.

570

571 QPCR for miRNA expression analysis was performed according to the primer
572 probe set manufacturers recommendations (ThermoFisher Scientific) and
573 using the TaqMan Universal PCR Master Mix (ThermoFisher Scientific, Cat#
574 4304437) with the same cycling scheme as above. Primer and probe sets for
575 TaqMan were also purchased from ThermoFisher Scientific (Life
576 Technologies at time of purchase, TaqMan® MicroRNA Assay, hsa-miR-34a,
577 human, Cat# 4440887, Assay ID: 000426 and Control miRNA Assay, RNU48,
578 human, Cat# 4440887, Assay ID: 001006).

579

580 The $\Delta\Delta Ct$ method was used to quantify gene expression. All QPCR-based
581 experiments were performed in at least technical duplicate. Primers for all
582 PCR-based experiments are listed in **Supplementary Document 2** and
583 arranged by figure.

584

585 **Cell Cycle Distribution**

586 Cells were washed in PBS and fixed in 4% paraformaldehyde at room
587 temperature overnight. Paraformaldehyde was removed, and cells were re-
588 suspended in 95% EtOH. The samples were then rehydrated in distilled
589 water, stained with DAPI and analyzed by flow cytometry on a LSRII (BD
590 Biosciences) machine. Resulting cell cycle phases were quantified using the

591 ModFit software (Verity Software House, Topsham, ME, USA). Experiments
592 were performed in biological quadruplet (PC3) or triplicate (Skov3). The log₂
593 fraction of cell cycle phase was calculated for each replicate a two sample t-
594 test was utilized for statistical testing.

595

596 **3' Rapid Amplification of cDNA Ends**

597 3'-RACE was performed as described as previously in (Johnsson et al. 2013).
598 Briefly, U2OS cell RNA was polyA-tailed using yeast polyA polymerase
599 (ThermoFisher Scientific, Cat# 74225Z25KU) after which cDNA was
600 synthesized using oligo(dT) primers. Nested-PCR was performed first using a
601 forward primer in miR34a asRNA exon 1 and a tailed oligo(dT) primer
602 followed by a second PCR using an alternate miR34a asRNA exon 1 primer
603 and a reverse primer binding to the tail of the previously used oligo(dT)
604 primer. PCR products were gel purified and cloned the Strata Clone Kit
605 (Agilent Technologies, Santa Clara, CA, USA. Cat# 240205), and sequenced.

606

607 **Chromatin Immunoprecipitation**

608 The ChIP was performed as previously described in (Johnsson et al. 2013)
609 with the following modifications. Cells were crosslinked in 1% formaldehyde
610 (Merck, Cat# 1040039025), quenched with 0.125M glycine (Sigma Aldrich,
611 Cat# G7126), and lysed in cell lysis buffer comprised of: 5mM PIPES (Sigma
612 Aldrich, Cat# 80635), 85mM KCL (Merck, Cat# 4936), 0.5% NP40 (Sigma
613 Aldrich, Cat# I8896), protease inhibitor (Roche Diagnostics, Cat#
614 004693159001). Samples were then sonicated in 50mM TRIS-HCL pH 8.0
615 (Sigma Aldrich, MO, USA, Cat# T2663) 10mM EDTA (Promega, WI, USA,

616 Cat# V4231), 1% SDS (ThermoFisher Scientific, Cat# AM9822), and protease
617 inhibitor (Roche Diagnostics, Cat# 004693159001) using a Bioruptor
618 Sonicator (Diagenode, Denville, NJ, USA). Samples were incubated over
619 night at 4°C with the *polII* antibody (Abcam, Cambridge, UK, Cat# ab5095)
620 and subsequently pulled down with Salmon Sperm DNA/Protein A Agarose
621 (Millipore, Cat# 16-157) beads. DNA was eluted in an elution buffer of 1%
622 SDS (ThermoFisher Scientific, Cat# AM9822) 100mM NaHCO3 (Sigma
623 Aldrich, Cat# 71631), followed by reverse crosslinking, RNaseA
624 (ThermoFisher Scientific, Cat# 1692412) and protease K (New England
625 Biolabs, Ipswich, MA, USA, Cat# P8107S) treatment. The DNA was eluted
626 using Qiagen PCR purification kit (Cat# 28106) and quantified via QPCR.
627 QPCR was performed in technical duplicate using the standard curve method
628 and reported absolute values. The fraction of input was subsequently
629 calculated using the mean of the technical replicates followed by calculating
630 the fold over the control condition. Statistical testing was performed using 4
631 biological replicates with the null hypothesis that the true log 2 fold change
632 values were equal to zero.

633

634 **Confluency Analysis**

635 Cells were incubated in the Spark Multimode Microplate (Tecan, Männedorf,
636 Switzerland) reader for 48 hours at 37°C with 5% CO₂ in a humidity chamber.
637 Confluency was measured every hour using bright-field microscopy and the
638 percentage of confluency was reported via the plate reader's inbuilt algorithm.
639 Percentage of confluency was normalized to the control sample in each
640 condition (shown in figure) and then ranked to move the data to a linear scale.

641 Using the mean of the technical duplicates in three biological replicates, the
642 rank was then used to construct a linear model, of the dependency of the rank
643 on the time and cell lines variables for each growth condition. Reported p-
644 values are derived from the t-test, testing the null hypothesis that the
645 coefficient estimate of the cell line variable is equal to 0.

646

647 **Pharmacological Compounds**

648 Doxorubicin was purchased from Teva (Petah Tikva, Israel, cat. nr. 021361).

649

650 **Cellular Localization Analysis**

651 Quantified RNAseq data from 11 cell lines from the GRCh38 assembly was
652 downloaded from the ENCODE project database and quantifications for
653 miR34a asRNA (ENSG00000234546), GAPDH (ENSG00000111640), and
654 MALAT1 (ENSG00000251562) were extracted. Cell lines for which data was
655 downloaded include: A549, GM12878, HeLa-S3, HepG2, HT1080, K562
656 MCF-7, NCI-H460, SK-MEL-5, SK-N-DZ, SK-N-SH. Initial exploratory analysis
657 revealed that several cell lines should be removed from the analysis due to a)
658 a larger proportion of GAPDH in the nucleus than cytoplasm or b) variation of
659 miR34a asRNA expression is too large to draw conclusions, or c) they have
660 no or low (<6 TPM) miR34a asRNA expression. Furthermore, only
661 polyadenylated libraries were used in the final analysis, due to the fact that
662 the cellular compartment enrichment was improved in these samples. All
663 analyzed genes are reported to be polyadenylated. In addition, only samples
664 with 2 biological replicates were retained. For each cell type, gene, and
665 biological replicate the fraction of transcripts per million (TPM) in each cellular

666 compartment was calculated as the fraction of TPM in the specific
667 compartment by the total TPM. The mean and standard deviation for the
668 fraction was subsequently calculated for each cell type and cellular
669 compartment and this information was represented in the final figure.

670

671 **CAGE Analysis**

672 All available CAGE data from the ENCODE project (Consortium 2012) for 36
673 cell lines was downloaded from the UCSC genome browser (Kent et al. 2002)
674 for genome version hg19. Of these, 28 cell lines had CAGE transcription start
675 sites (TSS) mapping to the plus strand of chromosome 1 and in regions
676 corresponding to 200 base pairs upstream of the *lnc34a* start site (9241796 -
677 200) and 200 base pairs upstream of the GENCODE
678 annotated *miR34a* asRNA start site (9242263 + 200). These cell lines
679 included: HFDPC, H1-hESC, HMEpC, HAoEC, HPIEpC, HSaVEC, GM12878,
680 hMSC-BM, HUVEC, AG04450, hMSC-UC, IMR90, NHDF, SK-N-SH_RA, BJ,
681 HOB, HPC-PL, HAoAF, NHEK, HVMF, HWP, MCF-7, HepG2, hMSC-AT,
682 NHEM.f_M2, SkMC, NHEM_M2, and HCH. In total 74 samples were included.
683 17 samples were polyA-, 47 samples were polyA+, and 10 samples were total
684 RNA. In addition, 34 samples were whole cell, 15 enriched for the cytosolic
685 fraction, 15 enriched for the nucleolus, and 15 enriched for the nucleus. All
686 CAGE transcription start sites were plotted and the RPKM of the individual
687 reads was used to color each read to indicate their relative abundance. In
688 cases where CAGE TSS spanned identical regions, the RPMKs of the regions
689 were summed and represented as one CAGE TSS in the figure. In addition, a
690 density plot shows the distribution of the CAGE reads in the specified

691 interval.

692

693 **Splice Junction Analysis**

694 All available whole cell (i.e. non-fractionated) spliced read data originating
695 from the Cold Spring Harbor Lab in the ENCODE project (Consortium 2012)
696 for 38 cell lines was downloaded from the UCSC genome browser (Kent et al.
697 2002). Of these cell lines, 36 had spliced reads mapping to the plus strand of
698 chromosome 1 and in the region between the *lnc34a* start (9241796) and
699 transcription termination (9257102) site (note that *miR34a* asRNA resides
700 totally within this region). Splice junctions from the following cell lines were
701 included in the final figure: A549, Ag04450, Bj, CD20, CD34 mobilized,
702 Gm12878, H1hesc, Haoaf, Haoec, Hch, Helas3, Hepg2, Hfdpc, Hmec,
703 Hmepc, Hmscat, Hmscbm, Hmscuc, Hob, Hpcpl, Hpiepc, Hsavec, Hsmm,
704 Huvec, Hvmf, Hwp, Imr90, Mcf7, Monocd14, Nhdf, Nhek, Nhemfm2,
705 Nhemm2, Nhlf, Skmc, and Sknsh. All splice junctions were included in the
706 figure and colored according to the number of reads corresponding to each. In
707 cases where identical reads were detected multiple times, the read count was
708 summed and represented as one read in the figure.

709

710 **TCGA Expression and Correlation Analysis**

711 Erik/Jimmy should probably take this.

712

713 **Acknowledgments**

714

715 **Competing Interests**

716

717 The authors declare no competing interests.

718

719 **Funding**

720
721 This work has been supported by the Swedish Research Council [521-2012-2037],
722 Swedish Cancer Society [150768], Cancer Research Foundations of Radiumhemmet
723 [144063] and the Swedish Childhood Cancer Foundation [PR2015-0009].

724

725

726 **Figure Supplements**

727

728 Figure 1-Supplement 1: TCAG expression levels and correlation analysis
729 statistics.

730

731 Figure 1-Supplement 2: Molecular characteristics of miR34a asRNA.

732

733 Figure 2-Supplement 1: A schematic representation of the p1 construct.

734

735 Figure 2-Supplement 2: Evaluating the effects of miR34a asRNA down-
736 regulation.

737

738 Figure 3-Supplement 1: Physiological relevance of miR34a asRNA
739 overexpression.

740

741 Figure 3-Supplement 2: Effects of miR34a asRNA overexpression on cyclin
742 D1.

743

744 Supplementary Document 1: Evaluating the relationship between miR34a
745 asRNA and lnc34a.

746

747 Supplementary Document 2: A table of primers used in this study.

748 **Supplementary Figures**

749

A)

cancer	all n	all rho	all p	TP53wt n	TP53wt rho	TP53wt p	TP53mut n	TP53mut rho	TP53mut p
ACC	10	5.52e-01	1.04e-01	10	5.52e-01	1.04e-01	NA	NA	NA
BLCA	228	5.15e-01	7.89e-17	134	4.53e-01	3.86e-08	94	4.27e-01	1.73e-05
BRCA Basal	42	5.74e-01	9.54e-05	10	6.24e-01	6.02e-02	32	5.74e-01	7.41e-04
BRCA Her2	44	1.47e-01	3.39e-01	12	2.24e-01	4.85e-01	32	6.82e-02	7.10e-01
BRCA LumA	199	3.41e-01	8.22e-07	177	3.43e-01	2.96e-06	22	4.86e-01	2.31e-02
BRCA LumB	70	1.71e-01	1.57e-01	61	1.48e-01	2.53e-01	9	1.67e-01	6.78e-01
CESC	156	1.39e-01	8.37e-02	145	1.60e-01	5.45e-02	11	-4.55e-02	9.03e-01
HNSC	313	5.37e-01	8.38e-25	123	6.08e-01	0.00e+00	190	4.47e-01	9.68e-11
KICH	5	6.00e-01	3.50e-01	5	6.00e-01	3.50e-01	NA	NA	NA
KIRC	142	3.49e-01	2.06e-05	141	3.37e-01	4.41e-05	NA	NA	NA
KIRP	167	4.51e-01	9.16e-10	163	4.48e-01	2.04e-09	4	8.00e-01	3.33e-01
LGG	271	6.33e-01	9.92e-32	76	7.28e-01	0.00e+00	195	3.87e-01	2.26e-08
LIHC	153	5.63e-01	3.64e-14	114	5.16e-01	4.18e-09	39	4.55e-01	3.95e-03
LUAD	234	2.82e-01	1.15e-05	128	3.61e-01	2.87e-05	106	2.27e-01	1.91e-02
LUSC	139	2.29e-01	6.74e-03	42	4.17e-02	7.93e-01	97	3.29e-01	9.91e-04
OV	56	2.33e-01	8.37e-02	10	8.42e-01	4.46e-03	46	1.46e-01	3.31e-01
PRAD	413	4.66e-01	1.33e-23	375	4.59e-01	6.13e-21	38	4.50e-01	4.58e-03
SKCM	165	6.48e-01	5.43e-21	152	6.10e-01	7.85e-17	13	4.34e-01	1.40e-01
STAD	225	3.72e-01	8.23e-09	145	3.67e-01	5.71e-06	80	4.20e-01	1.03e-04
THCA	469	4.58e-01	1.07e-25	467	4.62e-01	4.06e-26	NA	NA	NA

B)

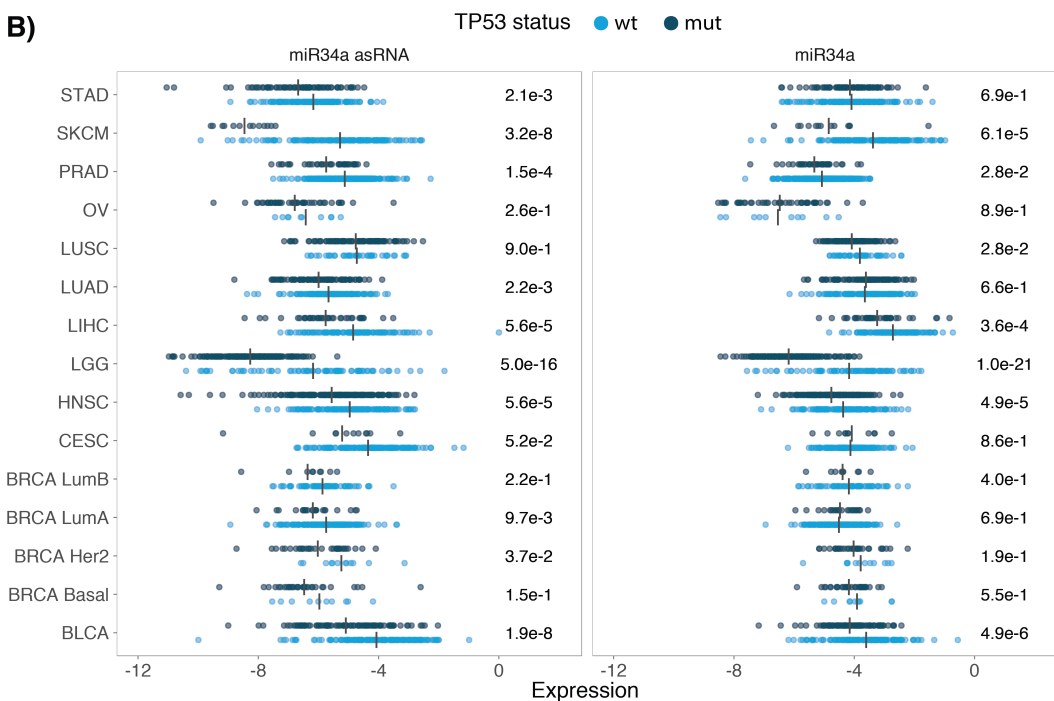
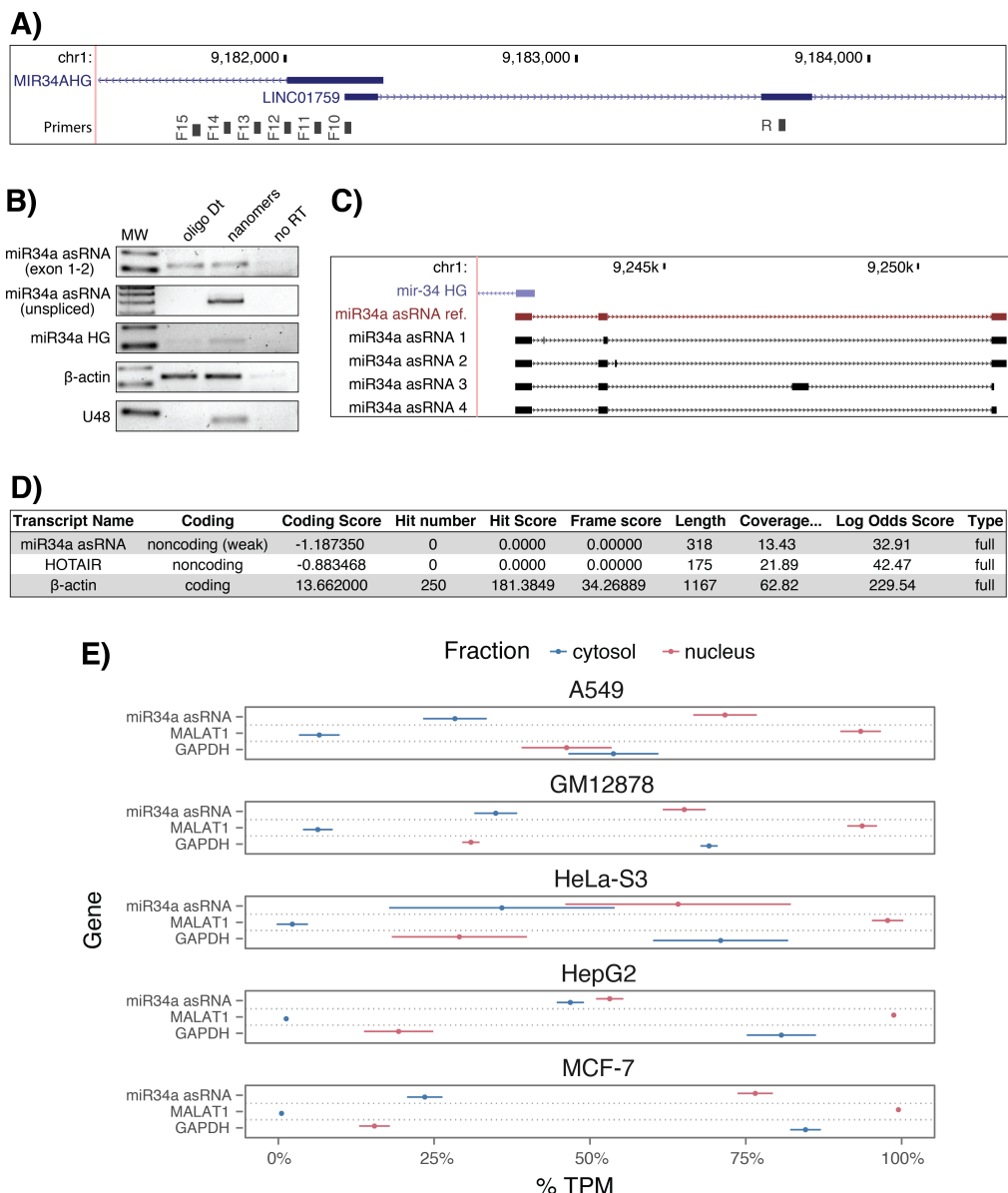


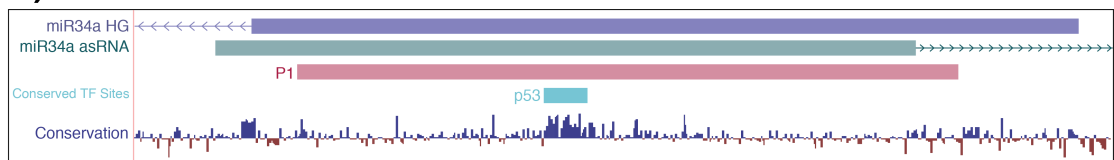
Figure 1 Supplement 1: TCAG expression levels and correlation analysis statistics. A) Spearman's rho and p-values (p) from the correlation analysis in Figure 1a. **B)** Expression levels of miR34a and miR34a asRNA in TP53 wt and nonsynonymous mutation samples. P-values are indicated on the right side of each panel are derived from comparing the TP53 wild type samples to the samples with a nonsynonymous mutation. Vertical lines indicate the mean. Bladder Urothelial Carcinoma (BLCA), Breast invasive carcinoma (BRCA), Head and Neck squamous cell carcinoma (HNSC), Lower Grade Glioma (LGG), Liver hepatocellular carcinoma (LIHC), Lung adenocarcinoma (LUAD), Lung squamous cell carcinoma (LUSC), Ovarian serous cystadenocarcinoma (OV), Prostate adenocarcinoma (PRAD), Skin Cutaneous Melanoma (SKCM), Stomach adenocarcinoma (STAD).



761
762
763
764
765
766
767
768
769
770
771
772
773

Figure 1 Supplement 2: Molecular characteristics of miR34a asRNA. **A)** A schematic representation of the primer placement in the primer walk assay. **B)** Polyadenylation status of spliced and unspliced miR34a asRNA in HEK293T cells. **C)** Sequencing results from the analysis of *miR34a* asRNA isoforms in U2OS cells. *miR34a* AS ref. refers to the full length transcript as defined by the 3'-RACE and primer walk assay. **D)** Analysis of coding potential of the *miR34a* asRNA transcript using the Coding-potential Calculator. **E)** RNAseq data from five fractionated cell lines in the ENCODE project showing the percentage of transcripts per million (TPM) for miR34a asRNA. MALAT1 (nuclear localization) and GAPDH (cytoplasmic localization) are included as fractionation controls. Points represent the mean and horizontal lines represent the standard deviation from two biological replicates.

A)

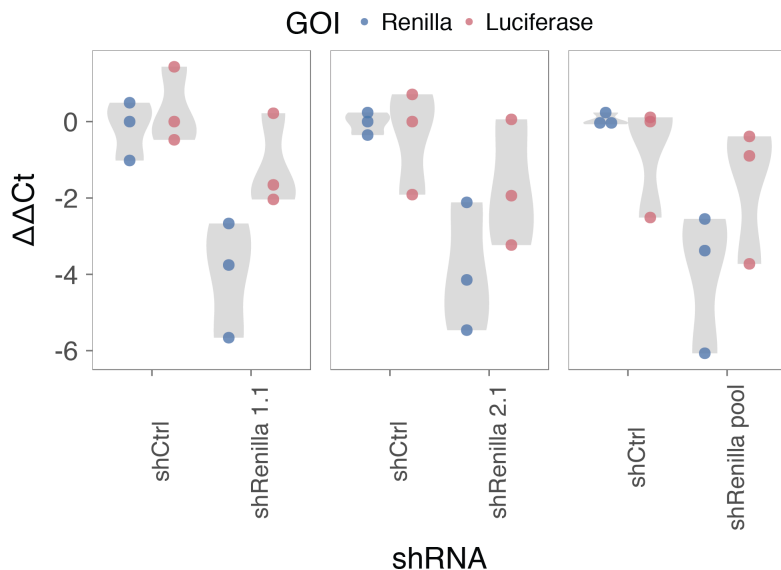


B)



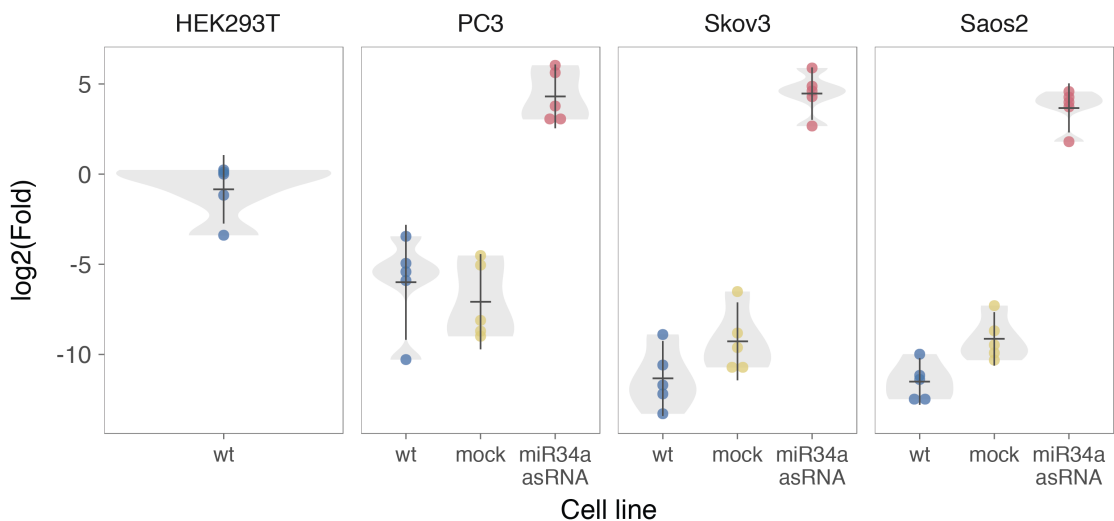
774
775
776
777
778
779

Figure 2 Supplement 1: A schematic representation of the p1 construct. A) A UCSC genome browser illustration indicating the location of the promoter region cloned into the p1 construct including the conserved *TP53*-binding site. **B)** A representative picture of the p1 construct including forward (F) and reverse (R) primer locations and the renilla shRNA targeting site.



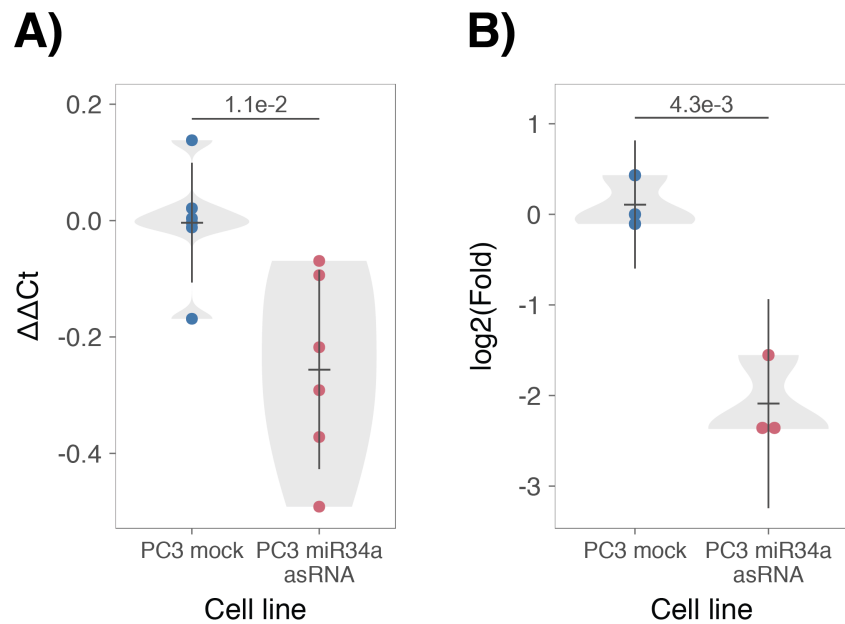
780
781
782
783
784
785
786

Figure 2 Supplement 2: Evaluating the effects of miR34a asRNA down-regulation. HEK293T cells were co-transfected with the P1 construct and either shRenilla or shControl. Renilla and luciferase levels were measured with Q-PCR 48 hours after transfection. Individual points represent independent experiments with the gray shadow indicating the density of the points. The experiment was performed in biological triplicate.



787
788
789
790
791

Figure 3 Supplement 1: Physiological relevance of miR34a asRNA overexpression. Comparison of *miR34a* asRNA expression in HEK293T cells (high endogenous *miR34a* asRNA), and the wild-type (wt), mock, and *miR34a* asRNA over-expressing stable cell lines.



792
793
794
795
796

Figure 3 Supplement 2: Effects of miR34a asRNA overexpression on cyclin D1. CCND1 expression (A) and western blot quantification of protein levels (B) in *miR34a* asRNA over-expressing PC3 stable cell lines. Experiments were performed in biological sextuplets (A) or triplicates (B).

797 **References**

- 798
- 799 Agostini, M., P. Tucci, R. Killick, E. Candi, B. S. Sayan, P. Rivetti di Val Cervo, P.
800 Nicotera, F. McKeon, R. A. Knight, T. W. Mak and G. Melino (2011). "Neuronal
801 differentiation by TAp73 is mediated by microRNA-34a regulation of synaptic
802 protein targets." *Proc Natl Acad Sci U S A* **108**(52): 21093-21098. DOI:
803 10.1073/pnas.1112061109
- 804
- 805 Ahn, Y. H., D. L. Gibbons, D. Chakravarti, C. J. Creighton, Z. H. Rizvi, H. P. Adams, A.
806 Pertsemlidis, P. A. Gregory, J. A. Wright, G. J. Goodall, E. R. Flores and J. M. Kurie
807 (2012). "ZEB1 drives prometastatic actin cytoskeletal remodeling by
808 downregulating miR-34a expression." *J Clin Invest* **122**(9): 3170-3183. DOI:
809 10.1172/JCI63608
- 810
- 811 Allaire, J., Y. Xie, J. McPherson, J. Luraschi, K. Ushey, A. Atkins, H. Wickham, J.
812 Cheng and W. Chang (2017). rmarkdown: Dynamic Documents for R. R package
813 version 1.8. <https://CRAN.R-project.org/package=rmarkdown>
- 814
- 815 Amarzguioui, M., J. J. Rossi and D. Kim (2005). "Approaches for chemically
816 synthesized siRNA and vector-mediated RNAi." *FEBS Lett* **579**(26): 5974-5981.
817 DOI: 10.1016/j.febslet.2005.08.070
- 818
- 819 Arnold, J. B. (2017). ggthemes: Extra Themes, Scales and Geoms for 'ggplot2'. R
820 package version 3.4.0. <https://CRAN.R-project.org/package=ggthemes>
- 821
- 822 Ashouri, A., V. I. Sayin, J. Van den Eynden, S. X. Singh, T. Papagiannakopoulos and
823 E. Larsson (2016). "Pan-cancer transcriptomic analysis associates long non-
824 coding RNAs with key mutational driver events." *Nature Communications* **7**:
825 13197. DOI: 10.1038/ncomms13197
- 826
- 827 Balbin, O. A., R. Malik, S. M. Dhanasekaran, J. R. Prensner, X. Cao, Y. M. Wu, D.
828 Robinson, R. Wang, G. Chen, D. G. Beer, A. I. Nesvizhskii and A. M. Chinnaian
829 (2015). "The landscape of antisense gene expression in human cancers." *Genome
830 Res* **25**(7): 1068-1079. DOI: 10.1101/gr.180596.114
- 831
- 832 Boque-Sastre, R., M. Soler, C. Oliveira-Mateos, A. Portela, C. Moutinho, S. Sayols, A.
833 Villanueva, M. Esteller and S. Guil (2015). "Head-to-head antisense transcription
834 and R-loop formation promotes transcriptional activation." *Proc Natl Acad Sci U
835 SA* **112**(18): 5785-5790. DOI: 10.1073/pnas.1421197112
- 836
- 837 Chang, T. C., D. Yu, Y. S. Lee, E. A. Wentzel, D. E. Arking, K. M. West, C. V. Dang, A.
838 Thomas-Tikhonenko and J. T. Mendell (2008). "Widespread microRNA
839 repression by Myc contributes to tumorigenesis." *Nat Genet* **40**(1): 43-50. DOI:
840 10.1038/ng.2007.30
- 841
- 842 Chang, W. (2014). extrafont: Tools for using fonts. R package version 0.17.
843 <https://CRAN.R-project.org/package=extrafont>
- 844

- 845 Chen, J., M. Sun, W. J. Kent, X. Huang, H. Xie, W. Wang, G. Zhou, R. Z. Shi and J. D.
846 Rowley (2004). "Over 20% of human transcripts might form sense-antisense
847 pairs." *Nucleic Acids Res* **32**(16): 4812-4820. DOI: 10.1093/nar/gkh818
- 848
- 849 Cheng, J., L. Zhou, Q. F. Xie, H. Y. Xie, X. Y. Wei, F. Gao, C. Y. Xing, X. Xu, L. J. Li and S.
850 S. Zheng (2010). "The impact of miR-34a on protein output in hepatocellular
851 carcinoma HepG2 cells." *Proteomics* **10**(8): 1557-1572. DOI:
852 10.1002/pmic.200900646
- 853
- 854 Chim, C. S., K. Y. Wong, Y. Qi, F. Loong, W. L. Lam, L. G. Wong, D. Y. Jin, J. F. Costello
855 and R. Liang (2010). "Epigenetic inactivation of the miR-34a in hematological
856 malignancies." *Carcinogenesis* **31**(4): 745-750. DOI: 10.1093/carcin/bgq033
- 857
- 858 Cole, K. A., E. F. Attiyeh, Y. P. Mosse, M. J. Laquaglia, S. J. Diskin, G. M. Brodeur and
859 J. M. Maris (2008). "A functional screen identifies miR-34a as a candidate
860 neuroblastoma tumor suppressor gene." *Mol Cancer Res* **6**(5): 735-742. DOI:
861 10.1158/1541-7786.MCR-07-2102
- 862
- 863 Conley, A. B. and I. K. Jordan (2012). "Epigenetic regulation of human cis-natural
864 antisense transcripts." *Nucleic Acids Res* **40**(4): 1438-1445. DOI:
865 10.1093/nar/gkr1010
- 866
- 867 Consortium, E. P. (2012). "An integrated encyclopedia of DNA elements in the
868 human genome." *Nature* **489**(7414): 57-74. DOI: 10.1038/nature11247
- 869
- 870 Ding, N., H. Wu, T. Tao and E. Peng (2017). "NEAT1 regulates cell proliferation
871 and apoptosis of ovarian cancer by miR-34a-5p/BCL2." *Onco Targets Ther* **10**:
872 4905-4915. DOI: 10.2147/OTT.S142446
- 873
- 874 Djebali, S., C. A. Davis, A. Merkel, A. Dobin, T. Lassmann, A. Mortazavi, A. Tanzer, J.
875 Lagarde, W. Lin, F. Schlesinger, C. Xue, G. K. Marinov, J. Khatun, B. A. Williams, C.
876 Zaleski, J. Rozowsky, M. Roder, F. Kokocinski, R. F. Abdelhamid, T. Alioto, I.
877 Antoshechkin, M. T. Baer, N. S. Bar, P. Batut, K. Bell, I. Bell, S. Chakrabortty, X.
878 Chen, J. Chrast, J. Curado, T. Derrien, J. Drenkow, E. Dumais, J. Dumais, R.
879 Duttagupta, E. Falconnet, M. Fastuca, K. Fejes-Toth, P. Ferreira, S. Foissac, M. J.
880 Fullwood, H. Gao, D. Gonzalez, A. Gordon, H. Gunawardena, C. Howald, S. Jha, R.
881 Johnson, P. Kapranov, B. King, C. Kingswood, O. J. Luo, E. Park, K. Persaud, J. B.
882 Preall, P. Ribeca, B. Risk, D. Robyr, M. Sammeth, L. Schaffer, L. H. See, A. Shahab, J.
883 Skancke, A. M. Suzuki, H. Takahashi, H. Tilgner, D. Trout, N. Walters, H. Wang, J.
884 Wrobel, Y. Yu, X. Ruan, Y. Hayashizaki, J. Harrow, M. Gerstein, T. Hubbard, A.
885 Reymond, S. E. Antonarakis, G. Hannon, M. C. Giddings, Y. Ruan, B. Wold, P.
886 Carninci, R. Guigo and T. R. Gingeras (2012). "Landscape of transcription in
887 human cells." *Nature* **489**(7414): 101-108. DOI: 10.1038/nature11233
- 888
- 889 Gallardo, E., A. Navarro, N. Vinolas, R. M. Marrades, T. Diaz, B. Gel, A. Quera, E.
890 Bandres, J. Garcia-Foncillas, J. Ramirez and M. Monzo (2009). "miR-34a as a
891 prognostic marker of relapse in surgically resected non-small-cell lung cancer."
892 *Carcinogenesis* **30**(11): 1903-1909. DOI: 10.1093/carcin/bgp219
- 893

- 894 Hunten, S., M. Kaller, F. Drepper, S. Oeljeklaus, T. Bonfert, F. Erhard, A. Dueck, N.
895 Eichner, C. C. Friedel, G. Meister, R. Zimmer, B. Warscheid and H. Hermeking
896 (2015). "p53-Regulated Networks of Protein, mRNA, miRNA, and lncRNA
897 Expression Revealed by Integrated Pulsed Stable Isotope Labeling With Amino
898 Acids in Cell Culture (pSILAC) and Next Generation Sequencing (NGS) Analyses."
899 Mol Cell Proteomics **14**(10): 2609-2629. DOI: 10.1074/mcp.M115.050237
- 900
- 901 International Human Genome Sequencing, C. (2004). "Finishing the euchromatic
902 sequence of the human genome." Nature **431**(7011): 931-945. DOI:
903 10.1038/nature03001
- 904
- 905 Johnsson, P., A. Ackley, L. Vidarsdottir, W. O. Lui, M. Corcoran, D. Grander and K.
906 V. Morris (2013). "A pseudogene long-noncoding-RNA network regulates PTEN
907 transcription and translation in human cells." Nat Struct Mol Biol **20**(4): 440-
908 446. DOI: 10.1038/nsmb.2516
- 909
- 910 Katayama, S., Y. Tomaru, T. Kasukawa, K. Waki, M. Nakanishi, M. Nakamura, H.
911 Nishida, C. C. Yap, M. Suzuki, J. Kawai, H. Suzuki, P. Carninci, Y. Hayashizaki, C.
912 Wells, M. Frith, T. Ravasi, K. C. Pang, J. Hallinan, J. Mattick, D. A. Hume, L. Lipovich,
913 S. Batalov, P. G. Engstrom, Y. Mizuno, M. A. Faghihi, A. Sandelin, A. M. Chalk, S.
914 Mottagui-Tabar, Z. Liang, B. Lenhard, C. Wahlestedt, R. G. E. R. Group, G. Genome
915 Science and F. Consortium (2005). "Antisense transcription in the mammalian
916 transcriptome." Science **309**(5740): 1564-1566. DOI: 10.1126/science.1112009
- 917
- 918 Kent, W. J., C. W. Sugnet, T. S. Furey, K. M. Roskin, T. H. Pringle, A. M. Zahler and D.
919 Haussler (2002). "The human genome browser at UCSC." Genome Res **12**(6):
920 996-1006. DOI: 10.1101/gr.229102. Article published online before print in May
921 2002
- 922
- 923 Kim, K. H., H. J. Kim and T. R. Lee (2017). "Epidermal long non-coding RNAs are
924 regulated by ultraviolet irradiation." Gene **637**: 196-202. DOI:
925 10.1016/j.gene.2017.09.043
- 926
- 927 Kong, L., Y. Zhang, Z. Q. Ye, X. Q. Liu, S. Q. Zhao, L. Wei and G. Gao (2007). "CPC:
928 assess the protein-coding potential of transcripts using sequence features and
929 support vector machine." Nucleic Acids Res **35**(Web Server issue): W345-349.
930 DOI: 10.1093/nar/gkm391
- 931
- 932 Lal, A., M. P. Thomas, G. Altschuler, F. Navarro, E. O'Day, X. L. Li, C. Concepcion, Y.
933 C. Han, J. Thiery, D. K. Rajani, A. Deutsch, O. Hofmann, A. Ventura, W. Hide and J.
934 Lieberman (2011). "Capture of microRNA-bound mRNAs identifies the tumor
935 suppressor miR-34a as a regulator of growth factor signaling." PLoS Genet **7**(11):
936 e1002363. DOI: 10.1371/journal.pgen.1002363
- 937
- 938 Leveille, N., C. A. Melo, K. Rooijers, A. Diaz-Lagares, S. A. Melo, G. Korkmaz, R.
939 Lopes, F. Akbari Moqadam, A. R. Maia, P. J. Wijchers, G. Geeven, M. L. den Boer, R.
940 Kalluri, W. de Laat, M. Esteller and R. Agami (2015). "Genome-wide profiling of
941 p53-regulated enhancer RNAs uncovers a subset of enhancers controlled by a
942 lncRNA." Nature Communications **6**: 6520. DOI: 10.1038/ncomms7520

943
944 Liu, C., K. Kelnar, B. Liu, X. Chen, T. Calhoun-Davis, H. Li, L. Patrawala, H. Yan, C.
945 Jeter, S. Honorio, J. F. Wiggins, A. G. Bader, R. Fagin, D. Brown and D. G. Tang
946 (2011). "The microRNA miR-34a inhibits prostate cancer stem cells and
947 metastasis by directly repressing CD44." *Nat Med* **17**(2): 211-215. DOI:
948 10.1038/nm.2284
949
950 Memczak, S., M. Jens, A. Elefsinioti, F. Torti, J. Krueger, A. Rybak, L. Maier, S. D.
951 Mackowiak, L. H. Gregersen, M. Munschauer, A. Loewer, U. Ziebold, M.
952 Landthaler, C. Kocks, F. le Noble and N. Rajewsky (2013). "Circular RNAs are a
953 large class of animal RNAs with regulatory potency." *Nature* **495**(7441): 333-
954 338. DOI: 10.1038/nature11928
955
956 O'Leary, N. A., M. W. Wright, J. R. Brister, S. Ciufo, D. Haddad, R. McVeigh, B.
957 Rajput, B. Robbertse, B. Smith-White, D. Ako-Adjei, A. Astashyn, A. Badretdin, Y.
958 Bao, O. Blinkova, V. Brover, V. Chetvernin, J. Choi, E. Cox, O. Ermolaeva, C. M.
959 Farrell, T. Goldfarb, T. Gupta, D. Haft, E. Hatcher, W. Hlavina, V. S. Joardar, V. K.
960 Kodali, W. Li, D. Maglott, P. Masterson, K. M. McGarvey, M. R. Murphy, K. O'Neill,
961 S. Pujar, S. H. Rangwala, D. Rausch, L. D. Riddick, C. Schoch, A. Shkeda, S. S. Storz,
962 H. Sun, F. Thibaud-Nissen, I. Tolstoy, R. E. Tully, A. R. Vatsan, C. Wallin, D. Webb,
963 W. Wu, M. J. Landrum, A. Kimchi, T. Tatusova, M. DiCuccio, P. Kitts, T. D. Murphy
964 and K. D. Pruitt (2016). "Reference sequence (RefSeq) database at NCBI: current
965 status, taxonomic expansion, and functional annotation." *Nucleic Acids Res*
966 **44**(D1): D733-745. DOI: 10.1093/nar/gkv1189
967
968 Ozsolak, F., P. Kapranov, S. Foissac, S. W. Kim, E. Fishilevich, A. P. Monaghan, B.
969 John and P. M. Milos (2010). "Comprehensive polyadenylation site maps in yeast
970 and human reveal pervasive alternative polyadenylation." *Cell* **143**(6): 1018-
971 1029. DOI: 10.1016/j.cell.2010.11.020
972
973 Polson, A., E. Durrett and D. Reisman (2011). "A bidirectional promoter reporter
974 vector for the analysis of the p53/WDR79 dual regulatory element." *Plasmid*
975 **66**(3): 169-179. DOI: 10.1016/j.plasmid.2011.08.004
976
977 Rashi-Elkeles, S., H. J. Warnatz, R. Elkon, A. Kupershtein, Y. Chobod, A. Paz, V.
978 Amstislavskiy, M. Sultan, H. Safer, W. Nietfeld, H. Lehrach, R. Shamir, M. L. Yaspo
979 and Y. Shiloh (2014). "Parallel profiling of the transcriptome, cistrome, and
980 epigenome in the cellular response to ionizing radiation." *Sci Signal* **7**(325): rs3.
981 DOI: 10.1126/scisignal.2005032
982
983 Raver-Shapira, N., E. Marciano, E. Meiri, Y. Spector, N. Rosenfeld, N. Moskovits, Z.
984 Bentwich and M. Oren (2007). "Transcriptional activation of miR-34a
985 contributes to p53-mediated apoptosis." *Mol Cell* **26**(5): 731-743. DOI:
986 10.1016/j.molcel.2007.05.017
987
988 Rinn, J. L., M. Kertesz, J. K. Wang, S. L. Squazzo, X. Xu, S. A. Brugmann, L. H.
989 Goodnough, J. A. Helms, P. J. Farnham, E. Segal and H. Y. Chang (2007).
990 "Functional demarcation of active and silent chromatin domains in human HOX

991 loci by noncoding RNAs." *Cell* **129**(7): 1311-1323. DOI:
992 10.1016/j.cell.2007.05.022
993
994 Rokavec, M., M. G. Oner, H. Li, R. Jackstadt, L. Jiang, D. Lodygin, M. Kaller, D. Horst,
995 P. K. Ziegler, S. Schwitalla, J. Slotta-Huspenina, F. G. Bader, F. R. Greten and H.
996 Hermeking (2015). "Corrigendum. IL-6R/STAT3/miR-34a feedback loop
997 promotes EMT-mediated colorectal cancer invasion and metastasis." *J Clin Invest*
998 **125**(3): 1362. DOI: 10.1172/JCI81340
999
1000 Schneider, C. A., W. S. Rasband and K. W. Eliceiri (2012). "NIH Image to ImageJ:
1001 25 years of image analysis." *Nat Methods* **9**(7): 671-675.
1002
1003 Serviss, J. T. (2017). miR34AasRNaproject.
1004 https://github.com/GranderLab/miR34a_asRNA_project
1005
1006 Serviss, J. T., P. Johnsson and D. Grander (2014). "An emerging role for long non-
1007 coding RNAs in cancer metastasis." *Front Genet* **5**: 234. DOI:
1008 10.3389/fgene.2014.00234
1009
1010 Slabakova, E., Z. Culig, J. Remsik and K. Soucek (2017). "Alternative mechanisms
1011 of miR-34a regulation in cancer." *Cell Death Dis* **8**(10): e3100. DOI:
1012 10.1038/cddis.2017.495
1013
1014 Stahlhut, C. and F. J. Slack (2015). "Combinatorial Action of MicroRNAs let-7 and
1015 miR-34 Effectively Synergizes with Erlotinib to Suppress Non-small Cell Lung
1016 Cancer Cell Proliferation." *Cell Cycle* **14**(13): 2171-2180. DOI:
1017 10.1080/15384101.2014.1003008
1018
1019 Su, X., D. Chakravarti, M. S. Cho, L. Liu, Y. J. Gi, Y. L. Lin, M. L. Leung, A. El-Naggar,
1020 C. J. Creighton, M. B. Suraokar, I. Wistuba and E. R. Flores (2010). "TAp63
1021 suppresses metastasis through coordinate regulation of Dicer and miRNAs."
1022 *Nature* **467**(7318): 986-990. DOI: 10.1038/nature09459
1023
1024 Sun, F., H. Fu, Q. Liu, Y. Tie, J. Zhu, R. Xing, Z. Sun and X. Zheng (2008).
1025 "Downregulation of CCND1 and CDK6 by miR-34a induces cell cycle arrest."
1026 *FEBS Lett* **582**(10): 1564-1568. DOI: 10.1016/j.febslet.2008.03.057
1027
1028 Tarasov, V., P. Jung, B. Verdoodt, D. Lodygin, A. Epanchintsev, A. Menssen, G.
1029 Meister and H. Hermeking (2007). "Differential regulation of microRNAs by p53
1030 revealed by massively parallel sequencing: miR-34a is a p53 target that induces
1031 apoptosis and G1-arrest." *Cell Cycle* **6**(13): 1586-1593. DOI:
1032 10.4161/cc.6.13.4436
1033
1034 Team, R. C. (2017). "R: A Language and Environment for Statistical Computing."
1035 from <https://www.R-project.org/>.
1036
1037 Turner, A. M., A. M. Ackley, M. A. Matrone and K. V. Morris (2012).
1038 "Characterization of an HIV-targeted transcriptional gene-silencing RNA in
1039 primary cells." *Hum Gene Ther* **23**(5): 473-483. DOI: 10.1089/hum.2011.165

- 1040
1041 Vogt, M., J. Mundig, M. Gruner, S. T. Liffers, B. Verdoodt, J. Hauk, L.
1042 Steinstraesser, A. Tannapfel and H. Hermeking (2011). "Frequent concomitant
1043 inactivation of miR-34a and miR-34b/c by CpG methylation in colorectal,
1044 pancreatic, mammary, ovarian, urothelial, and renal cell carcinomas and soft
1045 tissue sarcomas." *Virchows Arch* **458**(3): 313-322. DOI: 10.1007/s00428-010-
1046 1030-5
1047
1048 Wang, L., P. Bu, Y. Ai, T. Srinivasan, H. J. Chen, K. Xiang, S. M. Lipkin and X. Shen
1049 (2016). "A long non-coding RNA targets microRNA miR-34a to regulate colon
1050 cancer stem cell asymmetric division." *eLife* **5**. DOI: 10.7554/eLife.14620
1051
1052 Wang, L., H. J. Park, S. Dasari, S. Wang, J. P. Kocher and W. Li (2013). "CPAT:
1053 Coding-Potential Assessment Tool using an alignment-free logistic regression
1054 model." *Nucleic Acids Res* **41**(6): e74. DOI: 10.1093/nar/gkt006
1055
1056 Wang, X., J. Li, K. Dong, F. Lin, M. Long, Y. Ouyang, J. Wei, X. Chen, Y. Weng, T. He
1057 and H. Zhang (2015). "Tumor suppressor miR-34a targets PD-L1 and functions
1058 as a potential immunotherapeutic target in acute myeloid leukemia." *Cell Signal*
1059 **27**(3): 443-452. DOI: 10.1016/j.cellsig.2014.12.003
1060
1061 Wickham, H. (2016). gtable: Arrange 'Grobs' in Tables. R package version 0.2.0.
1062 <https://CRAN.R-project.org/package=gtable>
1063
1064 Wickham, H. (2017). scales: Scale Functions for Visualization. R package version
1065 0.5.0. <https://CRAN.R-project.org/package=scales>
1066
1067 Wickham, H. (2017). tidyverse: Easily Install and Load the 'Tidyverse'. R package
1068 version 1.2.1. <https://CRAN.R-project.org/package=tidyverse>
1069
1070 Wickham, L. H. a. H. (2017). rlang: Functions for Base Types and Core R and
1071 'Tidyverse' Features. R package version 0.1.4. [https://CRAN.R-project.org/package=rlang](https://CRAN.R-
1072 project.org/package=rlang)
1073
1074 Wickham, S. M. B. a. H. (2014). magrittr: A Forward-Pipe Operator for R. R
1075 package version 1.5. <https://CRAN.R-project.org/package=magrittr>
1076
1077 Wilkins, D. gggenes: Draw Gene Arrow Maps in 'ggplot2'. R package version
1078 0.2.0.9003. <https://github.com/wilkox/gggenes>
1079
1080 Xiao, N. (2017). liftr: Containerize R Markdown Documents. R package version
1081 0.7. <https://CRAN.R-project.org/package=liftr>
1082
1083 Xie, Y. (2017). knitr: A General-Purpose Package for Dynamic Report Generation
1084 in R. R package version 1.17. <https://yihui.name/knitr/>
1085
1086 Yang, P., Q. J. Li, Y. Feng, Y. Zhang, G. J. Markowitz, S. Ning, Y. Deng, J. Zhao, S.
1087 Jiang, Y. Yuan, H. Y. Wang, S. Q. Cheng, D. Xie and X. F. Wang (2012). "TGF-beta-
1088 miR-34a-CCL22 signaling-induced Treg cell recruitment promotes venous

1089 metastases of HBV-positive hepatocellular carcinoma." *Cancer Cell* **22**(3): 291-
1090 303. DOI: 10.1016/j.ccr.2012.07.023
1091
1092 Yap, K. L., S. Li, A. M. Munoz-Cabello, S. Raguz, L. Zeng, S. Mujtaba, J. Gil, M. J.
1093 Walsh and M. M. Zhou (2010). "Molecular interplay of the noncoding RNA ANRIL
1094 and methylated histone H3 lysine 27 by polycomb CBX7 in transcriptional
1095 silencing of INK4a." *Mol Cell* **38**(5): 662-674. DOI: 10.1016/j.molcel.2010.03.021
1096
1097 Yu, W., D. Gius, P. Onyango, K. Muldoon-Jacobs, J. Karp, A. P. Feinberg and H. Cui
1098 (2008). "Epigenetic silencing of tumour suppressor gene p15 by its antisense
1099 RNA." *Nature* **451**(7175): 202-206. DOI: 10.1038/nature06468
1100
1101 Zenz, T., J. Mohr, E. Eldering, A. P. Kater, A. Buhler, D. Kienle, D. Winkler, J. Durig,
1102 M. H. van Oers, D. Mertens, H. Dohner and S. Stilgenbauer (2009). "miR-34a as
1103 part of the resistance network in chronic lymphocytic leukemia." *Blood* **113**(16):
1104 3801-3808. DOI: 10.1182/blood-2008-08-172254
1105
1106
1107
1108